Temporally focused femtosecond laser pulses for low numerical aperture micromachining through optically transparent materials

Dawn N. Vitek,[1] Daniel E. Adams,[1] Adrea Johnson,[1] Philbert S. Tsai,[2] Sterling Backus,[3] Charles G. Durfee,[1] David Kleinfeld,[2] and Jeffrey A. Squier[1,*]

[1]*Center for Micro-integrated Optics for Advanced Bio-imaging and Control, Department of Physics, Colorado School of Mines, Golden, Colorado 80401, USA*
[2]*Department of Physics, University of California at San Diego, La Jolla, California 92093, USA*
[3]*Kapteyn-Murnane Laboratories, Inc., Boulder, Colorado 80301, USA*
**jsquier@mines.edu*

Abstract: Temporal focusing of spatially chirped femtosecond laser pulses overcomes previous limitations for ablating high aspect ratio features with low numerical aperture (NA) beams. Simultaneous spatial and temporal focusing reduces nonlinear interactions, such as self-focusing, prior to the focal plane so that deep (~1 mm) features with parallel sidewalls are ablated at high material removal rates (25 μm^3 per 80 μJ pulse) at 0.04-0.05 NA. This technique is applied to the fabrication of microfluidic devices by ablation through the back surface of thick (6 mm) fused silica substrates. It is also used to ablate bone under aqueous immersion to produce craniotomies.

OCIS codes: (230.4000) Microstructure fabrication; (140.3390) Laser materials processing; (190.4360) Nonlinear optics, devices; (170.1020) Ablation of tissue.

References

1. A. P. Joglekar, H. H. Liu, E. Meyhöfer, G. Mourou, and A. J. Hunt, "Optics at critical intensity: applications to nanomorphing," Proc. Natl. Acad. Sci. U.S.A. **101**(16), 5856–5861 (2004).
2. M. K. Bhuyan, F. Courvoisier, P.-A. Lacourt, M. Jacquot, L. Furfaro, M. J. Withford, and J. M. Dudley, "High aspect ratio taper-free microchannel fabrication using femtosecond Bessel beams," Opt. Express **18**(2), 566–574 (2010).
3. D. Schafer, E. A. Gibson, E. A. Salim, A. E. Palmer, R. Jimenez, and J. Squier, "Microfluidic cell counter with embedded optical fibers fabricated by femtosecond laser ablation and anodic bonding," Opt. Express **17**(8), 6068–6073 (2009).
4. Y. Li, K. Itoh, W. Watanabe, K. Yamada, D. Kuroda, J. Nishii, and Y. Y. Jiang, "Three-dimensional hole drilling of silica glass from the rear surface with femtosecond laser pulses," Opt. Lett. **26**(23), 1912–1914 (2001).
5. D. J. Hwang, T. Y. Choi, and C. P. Grigoropoulos, "Liquid-assisted femtosecond laser drilling of straight and three-dimensional microchannels in glass," Appl. Phys., A Mater. Sci. Process. **79**(3), 605–612 (2004).
6. D. Oron, E. Tal, and Y. Silberberg, "Scanningless depth-resolved microscopy," Opt. Express **13**(5), 1468–1476 (2005).
7. G. Zhu, J. van Howe, M. Durst, W. Zipfel, and C. Xu, "Simultaneous spatial and temporal focusing of femtosecond pulses," Opt. Express **13**(6), 2153–2159 (2005).
8. D. Vitek, D. Adams, A. Johnson, D. Kleinfeld, S. Backus, C. Durfee, and J. Squier, "Spatially chirped pulses for high aspect ratio micromachining by femtosecond laser ablation," in *Conference on Lasers and Electro-Optics/International Quantum Electronics Conference*, OSA T echnical Digest Series (CD) (Optical Society of America, 2010), paper CMBB5.
9. F. He, H. Xu, Y. Cheng, J. Ni, H. Xiong, Z. Xu, K. Sugioka, and K. Midorikawa, "Fabrication of microfluidic channels with a circular cross section using spatiotemporally focused femtosecond laser pulses," Opt. Lett. **35**(7), 1106–1108 (2010).
10. G. Veshapidze, M. L. Trachy, M. H. Shah, and B. D. DePaola, "Reducing the uncertainty in laser beam size measurement with a scanning edge method," Appl. Opt. **45**(32), 8197–8199 (2006).
11. J.-C. M. Diels, J. J. Fontaine, I. C. McMichael, and F. Simoni, "Control and measurement of ultrashort pulse shapes (in amplitude and phase) with femtosecond accuracy," Appl. Opt. **24**(9), 1270–1282 (1985).
12. M. A. Coughlan, M. Plewicki, and R. J. Levis, "Parametric spatio-temporal control of focusing laser pulses," Opt. Express **17**(18), 15808–15820 (2009).
13. J. F. Edd, D. D. Di Carlo, K. J. Humphry, S. Köster, D. Irimia, D. A. Weitz, and M. Toner, "Controlled encapsulation of single-cells into monodisperse picolitre drops," Lab Chip **8**(8), 1262–1264 (2008).

#130931 - $15.00 USD Received 1 Jul 2010; revised 2 Aug 2010; accepted 3 Aug 2010; published 6 Aug 2010

14. D. E. Hertzog, X. Michalet, M. Jäger, X. Kong, J. G. Santiago, S. Weiss, and O. Bakajin, "Femtomole mixer for microsecond kinetic studies of protein folding," Anal. Chem. **76**(24), 7169–7178 (2004).
15. M. Castaño-Álvarez, D. F. Pozo Ayuso, M. García Granda, M. T. Fernández-Abedul, J. Rodríguez García, and A. Costa-García, "Critical points in the fabrication of microfluidic devices on glass substrates," Sens. Actuators B Chem. **130**(1), 436–448 (2008).
16. P. S. Tsai, P. Blinder, B. J. Migliori, J. Neev, Y. Jin, J. A. Squier, and D. Kleinfeld, "Plasma-mediated ablation: an optical tool for submicrometer surgery on neuronal and vascular systems," Curr. Opin. Biotechnol. **20**(1), 90–99 (2009).
17. J. Neev, W. A. Carrasco, W. B. Armstrong, L. B. Da Silva, M. D. Feit, D. L. Matthews, M. D. Perry, A. M. Rubenchik, and B. C. Stuart, "Applications of ultrashort pulse lasers for hard tissue surgery," IEEE J. Sel. Top. Quantum Electron. **2**, 790–800 (1996).
18. P. S. Tsai, B. Friedman, A. I. Ifarraguerri, B. D. Thompson, V. Lev-Ram, C. B. Schaffer, Q. Xiong, R. Y. Tsien, J. A. Squier, and D. Kleinfeld, "All-optical histology using ultrashort laser pulses," Neuron **39**(1), 27–41 (2003).

1. Introduction

Micromachining with femtosecond laser pulses, in which the transient generation of a plasma leads to the ablation of material [1], is a powerful technique to cut chemically inert media such as glass. This procedure uniquely facilitates the prototyping of three-dimensional (3D) microanalytic devices with sub-diffraction-limited features. However, single-step processing has been limited in the size and aspect ratio of the features that can reasonably be produced in these media. As examples, in most fabrication techniques a laser beam is focused on the front surface of the substrate and ablation proceeds from the top down. Thus, successive pulses must focus through debris created by earlier pulses, and the pulses ultimately interact with the walls of the structure as the feature becomes deeper. This leads to a tapering of the feature that limits the aspect ratio [2,3].

An improved machining method would enable processing to take place through the *backside* of the wafer. Machining in this manner means that successive pulses would no longer focus through debris, nor interact with the walls, and thus makes it possible to produce exceptionally high aspect ratio features. Li *et al*. ablated high aspect ratio structures on the back surface of 1 mm thick glass at high numerical aperture (0.55 NA) [4]. The working distance was extended by Hwang *et al*., who employed a long working distance objective at 0.42 NA [5]. Bhuyan *et al*. achieved high aspect ratio structures with Bessel beams by focusing on the backside of the substrate [2]. However, Bessel beams do not have the same 3D control as other techniques. An improvement to backside machining would be to use lower NA beams in order to increase the interaction volume but without compromising 3D spatial confinement.

A high rate of cutting is crucial for applications wherein a significant volume of material must be ablated. For example, microfluidic devices require networks of channels that extend centimeters in length and laser surgery involves the removal of many cubic millimeters of material. A high rate of cutting appropriate for such applications is achieved by the introduction of temporal focusing, inspired by the work of Oron *et al*. [6] and Zhu *et al* [7]. In this technique, spatial chirping is used to form a frequency-distributed array of low NA beamlets, which coalesce to reform a transform-limited and diffraction-limited pulse at the focus of the objective. Oron *et al.* employed spatially chirped beams to effectively improve the axial sectioning in low NA, multiphoton imaging applications [6]. Zhu *et al*. showed that this technique reduces background excitation that is beneficial for multiphoton imaging in scattering media [7]. By adapting temporal focusing to our ablation beam, we are able to improve the machining rate and perform selective ablation through thick, optically transparent samples at 0.05 NA [8].

Temporally focused beams were employed by He *et al*. to write 2 mm long, sub-surface microfluidic channels and resulted in an improved channel shape [9]. We see similar gains in micromachining applications (Fig. 1). When 50 μJ, 60 fs, pulses (centered at 800 nm) are focused through a 6 mm thick fused silica sample at 0.05 NA without temporal focusing (Fig. 1(b)), we observe that the beam self-focuses and collapses into a filament. We are unable to selectively ablate the back surface of the sample, and the entire thickness of the glass is modified along the direction of propagation. Conversely, with temporal focusing and for the

#130931 - $15.00 USD Received 1 Jul 2010; revised 2 Aug 2010; accepted 3 Aug 2010; published 6 Aug 2010

same pulse energy and duration and focal spot size, we are able to selectively ablate only the back surface of the sample, leaving the glass volume nearly unblemished (Fig. 1(c)).

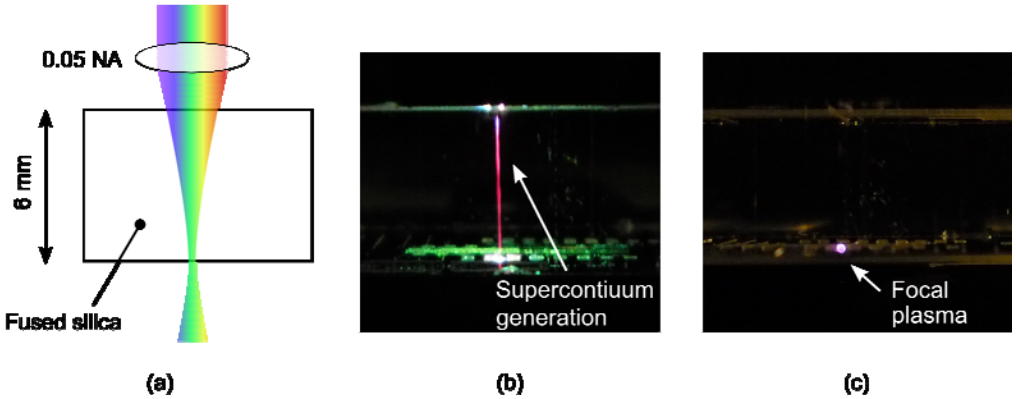

Fig. 1. Basic utility of temporal focusing for micromachining. (a) An illustration of the focusing geometry. 800 nm, 60 fs, 50 μJ pulses are focused at 0.05 NA at the back surface of a 6 mm thick block of fused silica. (b) Without spatially chirped pulses, self-focusing and supercontinuum generation result in a loss of intensity at the focus. The glass is tracked along the length of the filament and selective ablation at the focal depth is inhibited. (c) With spatially chirped pulses, self-focusing and continuum generation are suppressed, and the backside of the glass sample is ablated as evidenced by the plasma emission.

2. Experimental methods

We use a single-pass, double grating configuration to spatially chirp the beam. The input to the micromachining platform (Fig. 2) is positively chirped femtosecond pulses from a 1 kHz Ti:Al_2O_3 chirped pulse amplification system. The pulses must be slightly positively chirped to avoid pulse front tilt prior to the focusing element, given the single-pass, double grating configuration used to spatially chirp the beam. The grating system consists of two 600 l/mm gratings (Thorlabs, #GR25-0608) used at an angle of incidence of 36 degrees and a separation of 630 mm, as measured along the perpendicular between the gratings. The grating separation and angle are selected to minimize second and third order dispersion. Pulse compression is third-order limited as a result of the mismatch between the 1200 l/mm gratings in the laser compressor and the 600 l/mm gratings used to spatially chirp the beam. The net efficiency of the two 600 l/mm gratings is 50%. The radius of the beam incident on the focusing optic is 7.4 mm in the chirped dimension, as measured to the $1/e^2$ radius of the central intensity. In the unchirped dimension, the beam width is 0.69 mm at the $1/e^2$ radius. The beam is focused into the sample using a 25 mm focal length, 90-degree off-axis parabola (Janos Technology, #A8037-175). At focus the beam measured 33 μm at the $1/e^2$ radius in the direction of spatial chirp. Beam width measurements were made using the translating knife-edge method [10]. The pulse width at focus was measured with an interferometric second-order intensity autocorrelation [11] using a 100 μm thick KTP crystal and was determined to be 74 fs full-width at half maximum (FWHM) amplitude with the assumption of a hyperbolic secant pulse shape.

#130931 - $15.00 USD Received 1 Jul 2010; revised 2 Aug 2010; accepted 3 Aug 2010; published 6 Aug 2010

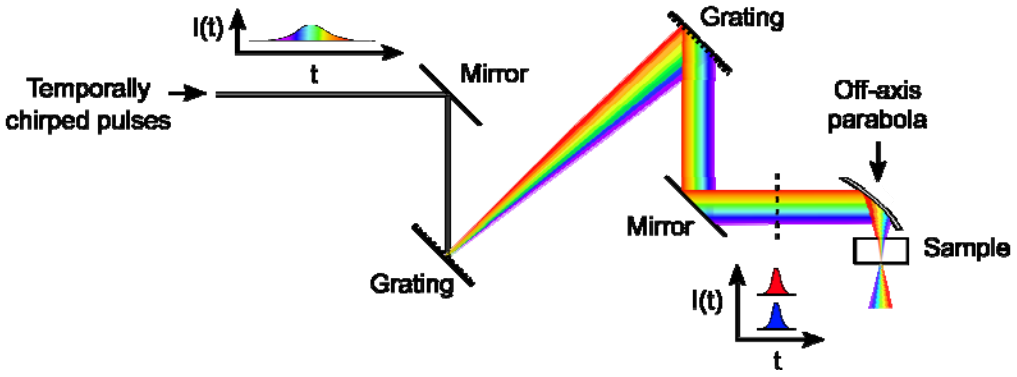

Fig. 2. Scheme for temporal focusing of chirped pulses. The temporally chirped pulses are spatially chirped then collimated by two gratings. After the second grating, the intensities, *I*, of all frequencies overlap in time, *t*, but the frequencies do not overlap spatially except at the focal plane.

We ablated channels and holes on the back surface of a 6 mm thick fused silica window with the use of an immersion setup (Fig. 3), similar to the setup in Hwang *et al*. [5]. Debris removal was aided by ultrasonic waves. The sample was mounted in a partially immersed glass chamber with 1 mm thick walls. Microfluidic channels were lengthened at a scan rate of 15 μm/s and deepened by 10 μm steps in the axial direction between scans. To determine the maximum aspect ratio of features, we machined holes in the back surface by scanning the sample axially at 10 μm/s.

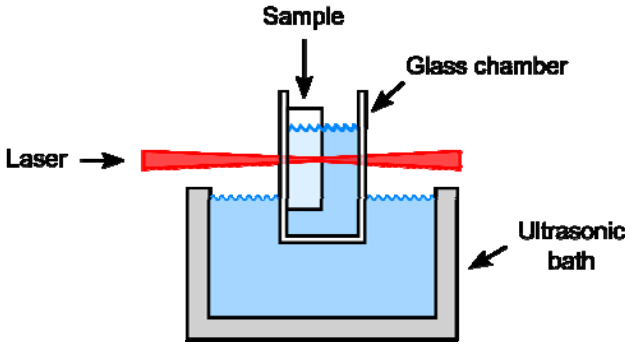

Fig. 3. The sample is mounted in a transparent glass chamber. The chamber is filled with water and partially immersed in an ultrasonic bath.

3. Simulations

An important quality of temporally focused pulses is a symmetric laser spot at the focus of the off-axis parabola. Ray-tracing (Fig. 4(a)) yields a diffraction-limited, round spot in focus and indicates that both the spatially chirped and non-spatially chirped dimensions of the beam focus to the same size (Fig. 4(b)). The symmetry of the focal spot was experimentally verified and is shown in Fig. 4(c). We also performed ray-tracing with 6 mm of fused silica placed before the focal plane as a means to simulate backside machining. The predicted focal spot is no longer symmetric. Dispersion from the fused silica stretched the focal spot along the spatially chirped dimension as different colors focused to slightly different lateral positions (Fig. 4(d)). The asymmetry was directly dependent on the thickness of the glass. With our beam parameters, a symmetric, diffraction-limited focal spot was predicted for fused silica samples less than ~2 mm thick.

#130931 - $15.00 USD Received 1 Jul 2010; revised 2 Aug 2010; accepted 3 Aug 2010; published 6 Aug 2010

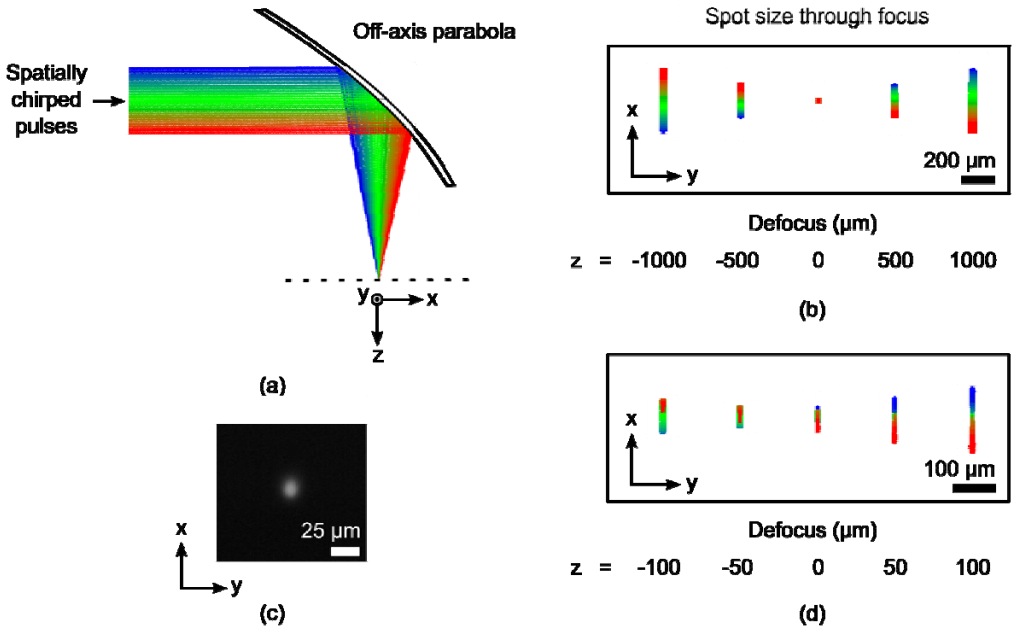

Fig. 4. Geometric optics model. (a) The beam was ray-traced through the focus of a 25 mm focal length, 90 degree off-axis parabola. The center wavelength and the FWHM edges of the spectrum were represented by green, blue and red rays, respectively. (b) The shape of the beam spot in *x* (chirped dimension) and *y* (unchirped dimension) was simulated at several axial positions through focus. At focus ($z = 0$) the beam spot was symmetric. (c) An image of the focal plasma in air. (d) The shape of the beam spot was asymmetric at focus with the addition of 6 mm of fused silica to simulate backside machining.

While ray-tracing provides details on the geometrical aspects of beam propagation that result from temporal focusing, we gain additional insight into the behavior of the laser pulses by calculating the spatio-temporal pattern of a pulse as it propagates through free space (Figs. 5,6). In particular, the pulse appears as a traveling wave that is transform-limited in time as well as diffraction-limited in space (Fig. 5(e)); see also Coughlan *et al.* [12].

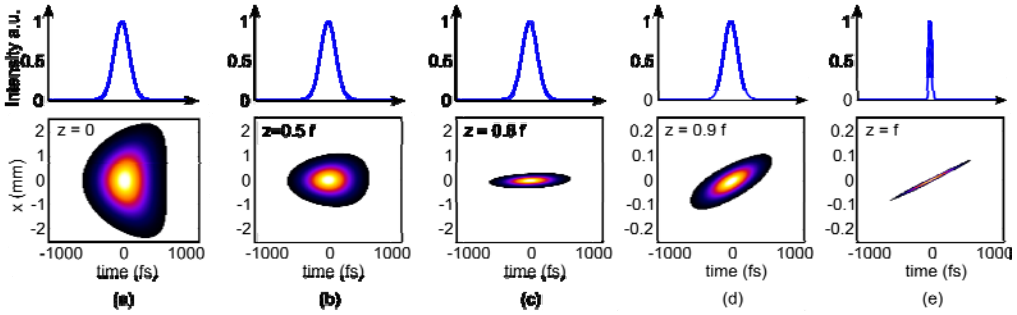

Fig. 5. Spatio-temporal beam propagation. Beam propagation was simulated in the spatially chirped dimension, *x*, generated by Fourier pulse propagation using the non-paraxial propagator. We begin from (a) the lens at $z = 0$ and proceed in (b)-(e) to the focal plane at $z = f$. Note that the spatial scale has changed between (c) and (d) by a factor of 10. Above each spatio-temporal plot is a lineout at $x = 0$ with a corresponding temporal axis.

The success of temporal focusing for backside micromachining lies with the improvement in the axial confinement and the reduction in the out-of-focus nonlinear interaction with the substrate. In Fig. 6 the depth of focus and the nonlinear phase accumulation, referred to as the *B*-integral, are plotted as a function of the spatial chirp. The degree of spatial chirp is given by the beam aspect ratio (BAR): the ratio of the spatially chirped beam diameter to the non-

#130931 - $15.00 USD Received 1 Jul 2010; revised 2 Aug 2010; accepted 3 Aug 2010; published 6 Aug 2010

spatially chirped beam diameter. The depth of focus is measured as the half width at half maximum (HWHM) amplitude of the axially dependent intensity profile. The peak value of the intensity was recorded for each axial position in the simulation. The HWHM was then calculated for the full peak-intensity profile, and this process was repeated for each value of the BAR. We observe that the *B*-integral steadily decreases as the BAR increases (inset to Fig. 6). For example, increasing the BAR from 4 to 8 results in more than a factor of 10 improvement. The BAR in our experiments was 11.

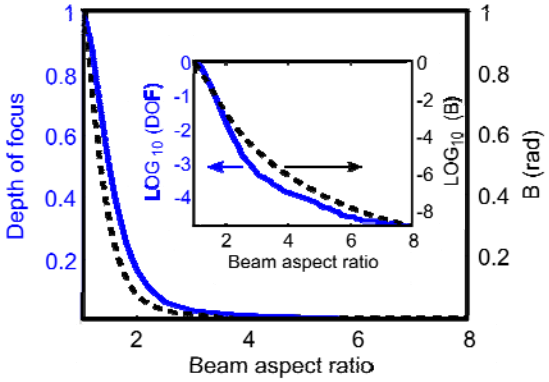

Fig. 6. The depth of focus (DOF) and the *B*-integral as a function of the beam aspect ratio. All quantities are scaled by the value for an unchirped beam (BAR = 1).

4. Results and discussion

We directly compared the channel aspect ratios obtained for backside and front side machining at low NA, with and without temporally focused pulses, respectively (Figs. 7(a), 7(b)). The image in Fig. 7(a) provides a 3D rendering of a channel ablated on the backside of the 6 mm fused silica sample. The image was collected with an Olympus OLS4000 confocal microscope. The channel was ablated at a rate of 25 μm^3 per 80 µJ pulse. The images in Figs. 7(c), 7(d) show side views of a deeper channel ablated on the back surface with the same machining parameters. The image in Fig. 7(b) shows a channel fabricated on the front surface without spatially chirped pulses, i.e., a conventional machining geometry. The most notable difference between the data in Figs. 7(a) and 7(b) is the slope of the sidewalls. The Olympus microscope was able to resolve indents sloped ≥5° from normal. The sloping of the channel walls for the microchannel fabricated on the front side was 22°. For the channel fabricated on the backside, the limit of 5° was reached indicating that the channels are sloped ≤5° from normal, i.e., the slope measurement is limited by the microscope.

#130931 - $15.00 USD Received 1 Jul 2010; revised 2 Aug 2010; accepted 3 Aug 2010; published 6 Aug 2010

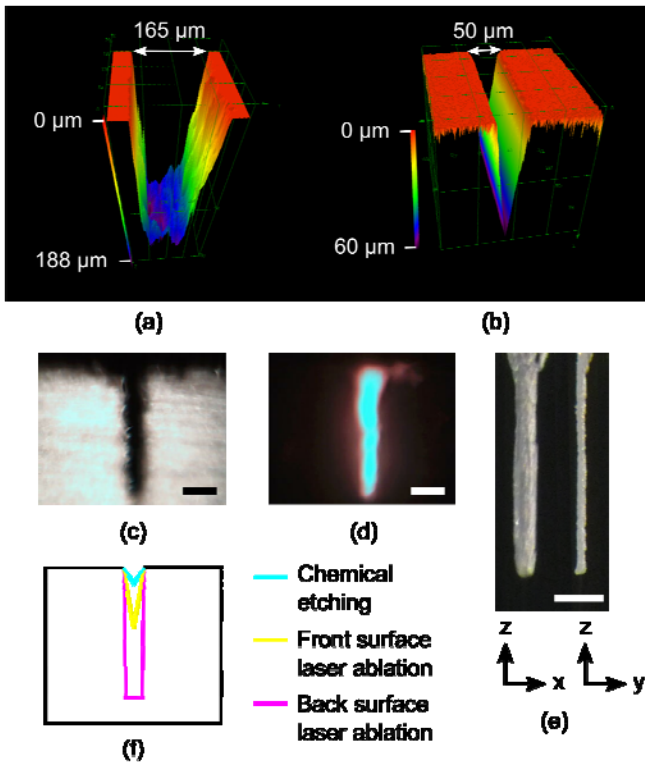

Fig. 7. Confocal images of 200 µm long segments of microfluidic channels cut on (a) the backside with temporal focusing at 0.04 NA and on (b) the front side without temporal focusing at 0.07 NA. (c,d) Side-view white light and fluorescence images of a microfluidic channel cut on the backside with temporal focusing. (e) A hole was ablated into the back surface and imaged from two angles: the spatially chirped dimension (left) and the unchirped dimension (right). (c-e) Scale bar, 200 µm. (f) An illustration comparing channel cross sections for chemical etching with our measurements for front surface laser ablation and for back surface laser ablation.

We investigated the maximum aspect ratio of features obtained with 100 µJ pulses by ablating holes into the back surface of the fused silica. The image in Fig. 7(e) shows a representative hole. We consistently saw a slight difference in morphology at the surface, and this was seen in both lateral dimensions. In addition, the shape of the ablated zone is wider in the chirped dimension. This is consistent with the asymmetric focal spot predicted by ray-tracing simulations due to dispersion from the fused silica sample (Fig. 4(d)). In the chirped dimension the aspect ratio is 10 (910 µm deep × 88 µm wide), and in the unchirped dimension the aspect ratio is 26 (910 µm deep × 35 µm wide). The maximum depth of the channel is directly affected by the effective removal of debris. Hwang *et al*. showed that immersion in a low viscosity fluid and introduction of ultrasonic waves improved the aspect ratio, and they drilled holes with aspect ratios up to 50 [5].

The ability to machine channels in glass with a high aspect ratio may benefit several types of microfluidic applications. Edd *et al*. implemented inertial focusing, a particle alignment technique, in channels with an aspect ratio of 2 in order to focus particles into one plane along the depth dimension [13]. Hertzog *et al*. designed a rapid microfluidic mixer for reaction dynamics studies where rapid mixing was achieved by squeezing reagents through a nozzle with an aspect ratio between 3 and 10, and dynamics were measured with confocal microscopy [14]. Even higher aspect ratio channels would be necessary for optical measurements that have a larger Rayleigh range, as is common for absorption measurements, to achieve mixing uniformity in the axial dimension. Neither Edd *et al*. nor Hertzog *et al*. used glass microfluidic devices. Many types of experiments in microfluidic devices may benefit

#130931 - $15.00 USD Received 1 Jul 2010; revised 2 Aug 2010; accepted 3 Aug 2010; published 6 Aug 2010

from the properties of glass. The mechanical strength of glass withstands pressure from the high flow rates used in inertial focusing and in rapid mixing. The chemical stability of glass is an advantage for chemical reaction studies, and the optical transparency of glass benefits white light imaging and absorption and fluorescence measurements.

The common fabrication approach for glass microfluidic devices, i.e., chemical etching, cannot yield the high aspect ratio channels required in these studies. Microfluidic channels fabricated by chemical etching have aspect ratios of less than one [15]. The illustration in Fig. 7(f) compares the aspect ratios in glass by chemical etching and low NA front and back surface laser ablation.

We now shift to the application of temporal focusing for the ablation of biological materials; see Tsai *et al.* for review [16]. Ablation with temporal focusing can potentially enable a variety of femtosecond laser surgeries, which were previously demonstrated with standard beams and under nonphysiological, dry conditions [17]. Studies of neuronal activity typically require thinning or removal of a portion of the skull to provide optical access to the brain. During this process, continual flushing with physiological saline is necessary to maintain tissue viability and to rinse away debris. Nonlinear interaction with the saline prohibits the use of low NA beams. However, with spatially chirped pulses and temporal focusing, rapid material removal under aqueous immersion is possible at low NA.

We performed a craniotomy on a mouse skull using plasma-mediated ablation with temporally focused pulses and the same set-up as for micromachining glass (Figs. 2,3). The skull was mounted in the center of the chamber with approximately 5 mm of water in the optical path. We removed a 1 mm × 2 mm × 0.3 mm section of the skull at a rate of 500 μm^3 per 130 µJ pulse or $2x10^6$ pulses per mm^3 (Fig. 8). The skull was removed in layers by sweeping laterally and then translating axially. The natural curvature of the skull allowed us to leave a portion of the skull intact after the final pass, thereby illustrating the axial confinement achieved by ablation with temporally focused pulses (Figs. 8(b), 8(c)). Additional passes would remove the remaining bone while minimizing ablation of underlying tissue. In this application, we ablated the sample on the front side under water. Ablation on the backside or in the interior of a transparent biological tissue should also be possible with consideration of the optical properties of the tissue, such as the shape and homogeneity, that may be expected to directly affect the quality of the focus.

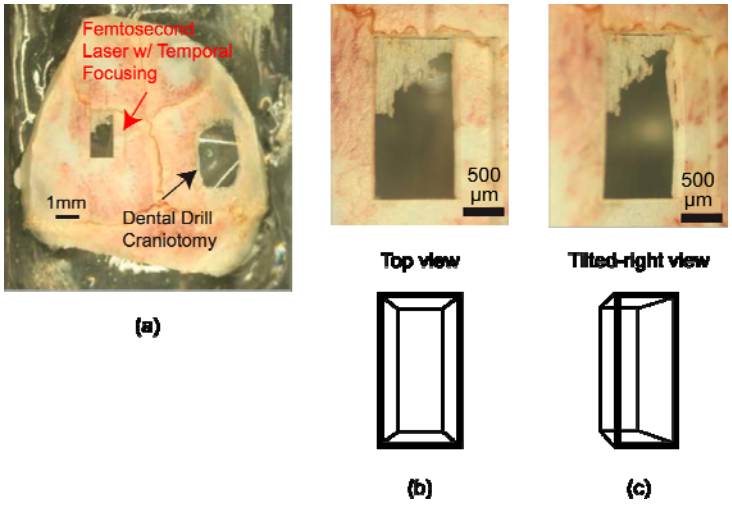

Fig. 8. (a) Craniotomy in an excised mouse skull performed using femtosecond laser ablation with spatially chirped pulses (on left). For comparison, we show a traditional craniotomy performed with a hand-held dental drill (on right). The 1 mm wide × 2 mm long × 0.3 mm deep craniotomy was produced with less than 20 minutes of laser ablation. (b) Top and (c) tilted-right enlarged views of the femtosecond laser craniotomy.

#130931 - $15.00 USD Received 1 Jul 2010; revised 2 Aug 2010; accepted 3 Aug 2010; published 6 Aug 2010

5. Conclusion

We have demonstrated the use of temporal focusing with low numerical aperture beams for femtosecond micromachining. This geometry mitigates nonlinear interactions such that material can be ablated through large path lengths of optically transparent material. We have shown that features with much higher aspect ratios can be produced using this technique compared with chemical etching. Although backside laser ablation is not the only technique for producing high aspect ratio channels in glass, it does add to the already extensive list of machining capabilities for femtosecond lasers in transparent materials, and, to our knowledge, it is the only single-step fabrication method for producing high aspect ratio channels in glass, which is especially useful for rapid prototyping.

High aspect ratio channels are essential for some types of microfluidic experiments that implement inertial focusing or rapid mixing, for example. With temporal focusing, we obtained aspect ratios up to 26. The aspect ratio was not the same in the spatially chirped and unchirped beam dimensions. This effect was consistent with simulations that predicted an elongated focal spot in the chirped dimension as a result of dispersion from the 6 mm thick fused silica substrate. This asymmetry is expected to increase for thicker samples, an important consideration for attaining high aspect ratio features in thick substrates. In principle, it is possible to precompensate for this chromatic aberration.

Machining at low NA results in a large volume of material removed per pulse. We demonstrated microfluidic channel machining rates of 25 μm^3 per 80 µJ pulse. However, the low repetition rate of our laser is prohibitive for fabricating complete microfluidic devices that typically consist of centimeters of channels. For example, at our demonstrated machining rate, 100 µm square microfluidic channels could be machined at a rate of one linear cm per hr. Clearly, higher repetition rate lasers are essential for full-scale microfluidic device fabrication, and these are commercially available. For example, a 100 kHz laser could machine the channel at a rate of 1.5 linear cm per min at the same pulse energy. This is an attractive machining rate for centimeter-scale microfluidic devices. In fact, this machining rate would surpass other methods such as fabrication by etching and/or lithography for many microfluidic channel geometries. Machining at low NA also improve the ablation rate of bone under aqueous immersion, and the same laser system should allow ablation of a cubic millimeter of bone in under one min. In general, we anticipate that femtosecond laser micromachining with temporal focusing may benefit other biomedical applications such as all optical histology [18] and deep tissue ablation in laser surgery [16].

Acknowledgments

We thank Charles V. Shank for insightful discussions that motivated this work. We gratefully acknowledge support for this work from the AFOSR (FA9550-07-10026 and FA9550-10-C-0017), the Colorado Bioscience Discovery Evaluation Grant Program, and the NIH (EB003832 and MH085499).

#130931 - $15.00 USD Received 1 Jul 2010; revised 2 Aug 2010; accepted 3 Aug 2010; published 6 Aug 2010